Signatures of Exo-solar Planets in Dust Debris Disks

Leonid M. Ozernoy[1]
5C3, Computational Sciences Institute and Department of Physics & Astronomy, George Mason U., Fairfax, VA 22030-4444; also Laboratory for Astronomy and Solar Physics, NASA/Goddard Space Flight Center, Greenbelt, MD 20771

Nick N. Gorkavyi[2]
NRC/NAS, Code 685, Laboratory for Astronomy and Solar Physics, Goddard Space Flight Center, Greenbelt, MD 20771

John C. Mather[3]
Code 685, Laboratory for Astronomy and Solar Physics, Goddard Space Flight Center, Greenbelt, MD 20771

and

Tanya A. Taidakova[4]
Computational Consulting Services, College Park, MD 20740

ABSTRACT

We have developed a new numerical approach to the dynamics of minor bodies and dust particles, which enables us to increase, without using a supercomputer, the number of employed particle positions in each model up to $10^{10} - 10^{11}$, a factor of $10^6 - 10^7$ higher than existing numerical simulations. We apply this powerful approach to the high-resolution modeling of the structure and emission of circumstellar dust disks, incorporating all relevant physical processes. In this *Letter*, we examine the resonant structure of a dusty disk induced by the presence of one planet of mass in the range of $(5 \cdot 10^{-5} - 5 \cdot 10^{-3})\ M_*$. It is shown that the planet, via resonances and gravitational scattering, produces (i) a central cavity void of dust; (ii) a trailing

[1]e-mail: ozernoy@science.gmu.edu; ozernoy@stars.gsfc.nasa.gov

[2]e-mail: gorkavyi@stars.gsfc.nasa.gov

[3]e-mail: john.c.mather@gsfc.nasa.gov

[4]e-mail: simeiz@aol.com

(sometimes leading) off-center cavity; and (iii) an asymmetric resonant dust belt with one, two, or more clumps. These features can serve as indicators of planet(s) embedded in the circumstellar dust disk and, moreover, can be used to determine the mass of the planet and even some of its orbital parameters. The results of our study reveal a remarkable similarity with various types of highly asymmetric circumstellar disks observed with the JCMT around Epsilon Eridani and Vega.

Subject headings: circumstellar matter–dust–planetary systems–stars: individual (ϵ Eridani, Vega)–

1. INTRODUCTION

1.1. Current approaches to the modeling of dusty disks and their limitations

Dusty disks around stars are a very common cosmic phenomenon (Beckwith & Sargent, 1993; Marcy, Cochran & Mayor, 1999; Woolf & Angel, 1998). Both the number and variety of circumstellar dusty disks being discovered by the HST and other telescopes grows swiftly, bringing new data virtually every month. These disks, with scales of tens to hundreds (up to a thousand) of AU, possess a great variety in structure, sometimes they have a central 'hole' void of gas and dust, and often are highly asymmetric. Those disks are thought to accompany planetary systems and, at the same time, to hide them from the observer. Knowledge of dust characteristics is of prime importance for future NASA's space missions, such as the NGST (Next Generation Space Telescope - see Mather et al. 1997) and the Terrestrial Planet Finder (TPF, 1999). It is generally expected that a significant limitation to unambiguous planet detection and study will be contaminating thermal emission from dust in the target systems. We propose to turn this hazard into an advantage for detecting and characterizing planetary systems.

The development of a detailed theoretical model of exo-zodiacal dust clouds is complicated by

- the wide variety of relevant physical processes, such as (i) dissipative effects (Poynting-Robertson drag, stellar wind, and aerodynamic drag), (ii) resonant interaction with planets, (iii) gravitational scattering by planets, (iv) evaporation and sputtering of dust particles, (v) mutual collisions in the cometary and dust populations, and
- uncertainties in the distribution of comets or other bodies as the major sources of dust in planetary systems.

Because of the complexity of the problem, the numerical approach is usually taken in modeling the IPD. Up until now, numerical models suffered from the limited number of particles that could be used in the computations. For instance, the first results in modeling dynamics of dust from the Kuiper belt were obtained by Liou, Zook, & Dermott (1996) with just 80 particles. Even now, numerical models treat several thousands of particles at most. While helpful in studying the dynamics of *individual dust particles*, these models cannot easily compute the large-scale structure of an IPD *cloud*, maps of the zodiacal emission of a circumstellar *disk*, etc.

1.2. Present Numerical Approach

Recently, we have proposed a novel, very effective approach to numerical modeling of distributions of test particles in an external gravitational field (Ozernoy, Gorkavyi, & Taidakova, 1998 ≡ OGT 1998), Gorkavyi, Ozernoy, Mather, & Taidakova ≡ GOMT 1999). In our approach, the particle-number limitation is solved, which is decisive to provide reliable numerical simulations. In brief, our approach (which has a number of common elements with the 'particle-in-cell' computational method) is as follows: Let us consider, for simplicity, a stationary (in the frame co-rotating with the planet) particle distribution. The locus of the given dust particle's positions (taken, say, as $6 \cdot 10^3$ positions every revolution about the star) are recorded and considered as the positions of *many other particles* produced by the same source of dust but *at a different time.* After this particle 'dies' (as a result of infall or ejection from the system by a planet-perturber), its recorded positions sampled over its lifetime form a stationary distribution as if it were produced by **many** particles. Typically, each run includes $10^4 - 10^5$ revolutions, i.e. $\sim 10^8$ positions of a dust particle, which is equivalent, for a stationary distribution, to 10^8 particles. If we allow for 100 sources of dust (we can include even a larger number of sources), we deal, after 100 runs, with $\sim 10^{10}$ particle positions as if they were real particles. This approach brings an factor of 10^6 improvement in the detail of a model! In the present Letter, we will not keep information about the dynamical path of each particle (as we did in OGT 1998 and GOMT 1998e), but instead, we will immediately sort this information into $8 \cdot 10^6$ spatial cells (each cell containing $10^3 - 10^4$ particles), thereby forming a 3D grid that models the dust cloud around the star (GOMT 1999). Our approach makes it possible to study, besides stationary processes, certain non-stationary processes as well, e.g. evolution toward steady-state distributions (OGT 1998, GOMT 1999), dust production from non-steady sources, decrease in particle size (due to evaporation) and number (due to collisions), etc.

In order to see the merits of our approach, we compare it, in Table 1, with that of Roques, Scholl, Sicardy, & Smith 1994 (hereinafter, RSSS), one of the best modeling of planetary dust disks so far. As can be seen, our approach offers greatly advanced opportunities for modeling circumstellar dust disks. In Sect. 2, we briefly duscuss the theoretical background. We explore the possible variety of dust disks with one embedded planet (Sect. 3) and then we make a preliminary interpretation of observations of certain circumstellar disks (Sect. 4). Our conclusions are given in in Sect. 5.

2. CIRCUMSTELLAR DISKS: THE ROLE OF RESONANCES

In the Solar system, the Kuiper belt objects ('kuiperoids'), along with comets and asteroids, serve as major sources of dust. These constituents are thought to be rather common for many circumstellar disks, which should contain not only planets but residual material such as kuiperoids, comets, and dust produced by these objects. Both the P-R and stellar wind drags (even stronger than in the Solar system whenever the star is more luminous) as well as residual gas in the disk tend to induce dust inflow toward the star. As the dust passes by the planets in its infall, it interacts with them by accumulating in the outer planetary resonances. Therefore, as we demonstrate below, the resonant structure in the dusty circumstellar disks could serve as an efficient means of planet detection.

2.1. Density Distribution of Dust in the Disk Without a Planet

It will be instructive to start with a limiting case of a circumnuclear disk composed only of sources of dust (no planets yet). We have computed a 3D model of such a disk produced by 25 kuiperoidal sources of dust experiencing the P-R drag. For illustrative purposes, the distribution of exo-kuiperods is taken similar to the kuiperoids in the Solar system. At distances from the star less than ca. 30 AU, the surface density of dust is found to be almost constant forming a plateau down the star, whereas the number density increases inward as $n_d \sim 1/r$. This result turns out to be in good accordance with our earlier analytical work (GOMT, 1997), which addressed the dust production by asteroids in the Solar system. Interestingly, the latter dependence differs substantially from that in the outer Solar system, where the presence of four giant planets results in $n_d \approx$ const (GOMT 1999).

2.2. Resonance Dust Rings Induced by Exo-planets

The major factor which makes visible the re-distribution of dust in the circumstellar disk due to the presense of embedded planet(s) are *resonances*. The existence of a resonance ring associated with the Earth's orbit was predicted by by Jackson & Zook (1989); such a ring was indeed discovered in the IRAS (Dermott et al. 1994) and COBE (Reach et al. 1995) data. Below, we focus on the conditions favorable to formation of resonant rings near the planetary orbits; this analytical consideration is very helpful in planning the numerical computations for a variety of environments.

2.2.1 Resonant capture

Weidenschilling and Jackson (1993) found a criterion for the resonant capture of particles into outer planetary resonances (2D case, the planet on a circular orbit): the capture into a resonance becomes possible for those resonances for which the gain in angular momentum is equal to the angular momentum loss due to dissipation, i.e. when the 'capture parameter' exceeds unity. This parameter depends upon the resonance number, the planetary mass, m_{pl}, orbital radius, and a value of $\beta \approx L_\star/(M_\star r)$, that is the ratio of the stellar light pressure and the gravitational force applied to the dust grain of radius r (in μm) ($L_\star$ and $M_\star$ being the star's luminosity and mass in solar units). Generally speaking, the 'capture parameter' depends also upon the eccentricity of the planet, e, and inclination of particles, i. For a given mass of the planet and size of dust particles, there are certain resonances favorable for the particle's capture: distant resonances are weaker and unable to intercept particles, whereas resonances close to a planet, which are stronger, do not get enough particles. The resonances determining the overall shape of a resonant ring and its asymmetry are entirely different for the Earth, which tends to capture particles into the resonances 6:5, ..., 11:10, etc., than for Neptune, which mainly captures particles into the resonances 2:1, 3:2, 4:3, etc., or Jupiter, whose major interceptors are the resonances 2:1, 3:1, 4:1, etc.

2.2.2 Resonant lifetime

Another important factor influencing the shape and structure of resonant belts is the dynamics of resonant particles, which can be characterized by the two closely related parameters: the lifetime spent in a resonance and the maximum eccentricity, $e_{\max}$, attained by a resonant particle. (The eccentricity grows due to the fact that the PR-drag decreases the particle's angular momentum even if the particle is stuck in a resonance, i.e. keeps its a = const). Besides an increase in e, the resonant particles change, in a complicated way, their i – cf. Liou & Zook (1997). Weidenschilling & Jackson (1993) found $e_{\max} = [0.4/(1+j)]^{1/2}$ (j being the resonance number), at which point, the pericenter of a particle's orbit becomes smaller than the planet's orbit ($q \approx 0.85 a_{pl}$) so that a further balance in angular momentum becomes impossible anymore and the particle leaves the resonance.

Dust particles captured into a resonance can reach $e \sim e_{\max}$ and spend an appreciable amount of time in this metastable state (Weidenschilling & Jackson 1993). Obviously, the appearance of this resonant belt only depends on a_{res} and $e_{\max}$, which are the same for all particles in the belt, regardless their initial a_0 and e_0.

For the Lindblad resonances $(j+1) : j$ as well as for the $j : 1$ resonances, which are of major interest to us, the lifetime of particles in the above metastable state rapidly

increases with the distance from the planet, whereas the probability of the resonant capture decreases. Hence, it would be a reasonable approximation to examine the contribution of various resonances into the the observed structure of the circumstellar disk by assuming that this structure is induced by just one of the outer resonances. Indeed, the outermost resonances are unable to capture particles, while the particle lifetime in the innermost resonances is much shorter. This approximation is employed in Sect. 4 when our simulated disks are compared with the observed circumstellar disks.

2.2.3 Mass of a Resonant Dusty Structure

The total mass of dust contained in the particular resonance is the product of the probability for the dust particle be captured into the resonance, the lifetime spent in the resonance, and the total dust flow per unit time in the vicinity of the resonance, i.e. $M_j = W_j \tau_j (\mathrm{d}M/\mathrm{d}t)$. Having introduced, for convenience, the mass of 'background' dust, M_b, which is common for all the resonances, one gets $M_j/M_b \approx W_j/(S_j - 1)(\tau_j/\tau_{PR})$, where S_j is the probability for the dust particle be ejected from the system due to gravitational scattering on the planet, and τ_{PR} is the characteristic time of the particle's semimajor axis change due to the Poynting-Robertson drag.

3. MODELLING CIRCUMSTELLAR DUST DISKS

We consider the simplest planetary system consisting of just one planet orbiting a star of mass $M \sim M_\odot$ and sitting at a eccentric orbit of a semi-major axis $a \sim 30$ AU. To explore the role of a particular resonance, we put the source of dust just outside of this resonance. Since the source of dust is assumed to belong to the Kuiper belt objects, its initial eccentricity and inclination were taken typical for kuiperoids (disk population): $e_0 \approx 0.07$ and $i_0 \approx 2 - 3°$. We have computed 40 model disks in order to explore the effects of various resonances adopting as parameters: (i) the mass of the planet; (ii) its orbital eccentricity; and (iii) particle size coupled with stellar luminosity and mass, as described by the parameter β, the ratio of the stellar light pressure and the gravitational force applied to the dust grain; $\beta \approx 0.3L/(Mr)$ depends upon the particle's radius r (in μm) and the star's luminosity L and mass M (in solar units) assuming dust grains of density 2 gcm^{-3}. Each model is based on just one run that reveals the distribution of dust particles between their capture into a resonance and eventual leaving it. (In fact, we explored 10 to 15 runs with various inital conditions and found the resulting distribution to be only slightly varying from one run to another. This confirms the conclusion reached at Sect. 2.2.2 that the appearance of a resonant belt is not sensitive to a_0 and e_0.) In those cases when the particle lifetime in the resonance was too long (exceeded $2 \cdot 10^6$ planet's revolutions, the run was stopped. This set of models was easily constructed, as the the CPU time to compute any

one model on a PC typically did not exceed a few hours (or dozens of hours for very small β's as well as very distant resonances). Below, we describe some of these models, in order to reveal the qualitative dependencies upon the above parameters.

3.1. Dependence of Structure Upon Particular Resonances

How one planet embedded into a circumstellar disk modifies its dust distribution through resonances, is shown in Figs. 1 and 2 as a set of 12 models that can be used to see the effects of different parameters. In each panel, the surface density of the disk is shown on a linear contrast scale; the area covered is 200x200 (scale is arbitrary but, for the Solar system, it would be in AU); and the (single) planet, at $r = 30$, is shown as the black square in Figs. 1 and 2 and as the white square in Fig. 3.

Fig. 1 illustrates the geometry of dust distribution in different mean motion resonances with the planet. One can see that the planet induces dramatic changes in dust distribution, compared to the structureless 'no planet' case (Sec. 2.1: (i) it creates a highly inhomogeneous resonant dust belt that forms near the planet's orbit, with belt's width that decreases as j increases; (ii) it works to clear from dust the central region within the planetary orbit; and (iii) it produces an additional highly asymmetric, banana-like empty region or a few such regions.

The above resonant dust belt consists of one or several clumps, which originate as follows. In a $m : n$ resonance, each particle experiences n passages through the pericenter while the planet makes m revolutions. In the rotating frame, the orbit of the resonant particle forms n loops in the vicinity of the planetary orbit. Since in the loop the particle moves relative to the planet rather slowly, the particle number density is enhanced there. If the amplitude of the azimuthal libration of particle orbits is small compared to the loop size, each loop produces one clump. In the opposite case of a large librational amplitude, each librating loop creates two clumps located in the two extreme points of libration. Thus, in a $m : n$ resonance, the number of clumps equals n at a small and $2n$ at a large libration. For instance, the 3:1 and 2:1 resonances each produce one clump (Figs. 2b and 2d), although, owing to libration, it is bifurcated as seen in Figs. 1a and 1b, 2a, 2c, and 2e); the 3:2 resonance yields four clumps (Fig. 1c); the 4:3 resonance gives six clumps (Fig. 1d); the 5:4 resonance produces eight clumps (Fig. 1e) and the 7:4 resonance - four clumps (Fig. 1f), etc.

Which of the above resonances is the 'strongest', in terms of the accumulated dust mass? The last equation of Sect. 2.2.3 enables us to obtain helpful estimates. For $\beta = 0.065$, one gets $\tau_{PR} \simeq 5 \cdot 10^4$ (hereinafter, time is measured in planet's revolutions, which is 160

yrs for a planet at 30 AU). According to our simulations, the lifetime in various resonances is as follows: $\tau_{4:3} \simeq 2 \cdot 10^4$; $\tau_{3:2} \simeq 5 \cdot 10^4$; $\tau_{2:1} \simeq 2.4 \cdot 10^5$; $\tau_{3:1} \simeq 8 \cdot 10^5$; $\tau_{4:1} > 2 \cdot 10^6$, etc. If, for simplicity, we put $W_j \simeq 1$ and neglect gravitational scattering of dust grains by the planet ($S_j \simeq 0$), we obtain as reasonable esimates that the dust structures in the resonances 4:3, 3:2, etc. are comparatively small ($M_j/M_b \lesssim 1$, whereas resonances 2:1, 3:1, etc. are very strong: $M_j/M_b \gg 1$. Since the probability of capture into the resonance $j:1$ decreases for larger j, the dust structures associated with the resonances 2:1 and 3:1 seem to happen rather often.

3.2. Dependence of Structure Upon Planetary Mass and Eccentricity

Given the resonance number, it interesting to examine how the planetary mass influences the distribution of dust. For the 2:1 resonance, Figs. 2 a,b and their comparison with Fig. 1b reveal that as m_{pl} increases, the banana-like empty region increases as well, whereas the angle at which the bifurcated substructure is seen from the star decreases: virtually one clump might be in the resonance 2:1 with the planet as massive as several m_J (Fig. 2b).

While taking into account all the resonances, influence of the planetary mass upon the dust structure is more complicated. Qualitatively, at $m_{pl}/M_\star \to 0$, it is very hard to capture dust particles into resonances. At m_{pl} small but finite, the captured particles are in a resonant ring, and if m_{pl} is as small as Earth the planet might be in a resonant lock with a trailing clump (Dermott et al. 1994, Reach et al. 1995, TPF 1999). One of the important new results of the present study is that the location of the density maximum in the wake, i.e. in the trailing zone of the planet, is only valid if the planetary mass is small enough; for masses larger, say, than that of Neptune, the density maximum, according to our simulations, is located in the leading zone (see Figs. 1 a,b,c,d and Fig. 2). The explanation and implications of this phenomenon are given elsewhere (GOM 1999). Here, we only notice that (i) depending upon resonance number, the clump(s) may be positioned differently relative to the planet - the latter is located either inside the zone of librational motion of the loop (Fig. 1e) or even within the loop - (Fig. 1f), and (ii) the leading clump becomes to be solitary one at the planetary mass as large as a few m_J (see Figs. 2b and 2d).

When the planetary mass is as large as $m \approx 5\ m_J$, it results in dust re-distribution in the circumstellar disk shown in Figs. 2 b,c,d. As is seen, the size of the clearing zone is appreciably larger, while the zone of libration is much smaller, so that the presence of a single clump becomes to be typical.

Finally, at $m_{pl} \gtrsim 10\ m_J$ or so dust again cannot be captured into a resonance such as

2:1 due to the overlapping of resonances (e.g. Wisdom 1980).

Important common features of the models shown in Figs. 1 and 2 include a clearing within the orbit of the planet and a banana-like empty region near the very planet (in its trailing zone). Dense resonant structures are characterized by richness in features and asymmetry. Figs. 1 and 2 give a clear indication of how the dust distribution in the disk changes as each of the parameters involved varies, influencing the most essential resonances and the number of dust particles captured into them. Asymmetry of the dust cloud changes its character for different values of β and is larger for smaller β. Therefore, if dust in circumstellar disks is stratified in particle's size, images of dusty disks should look differently, say, in IR and sub-mm wavelengths.

If the sources of dust are inner, gravitationally scattered comets (like those of Jupiter-family in the Solar system), their dust distribution differs drastically from that produced by external sources (kuiperoids). Using a stationary distribution of the simulated population of Jupiter-family comets computed by us elsewhere (OGT 1998), we can easily find the surface density of dust produced by this population . Since the pericenters of gravitationally scattered comets are usually located inside the planetary orbit , the dust produced by them easily penetrates deeply inside the system. This dust forms a disk-like cloud (rather then a belt, as in the case of outer, kuiperoidal sources), with the density of dust increasing steeply inward (GOMT 1997). The massive planet makes such a disk asymmetric: for instance, Jupiter's influence results in an arc along the resonant orbit 1:1.

4. A LINK TO OBSERVATIONS: IMAGERY OF CIRCUMSTELLAR DISKS

There are several points of comparison between our models and observations. The most direct comparison is of course the morphology or apparent structure of the disk. Besides, our models have implications for interpreting the IR to sub-mm spectral energy distributions (SED's) of circumstellar disks as observed by ISO or SCUBA with the JCM telescope. here, we consider some observational signatures of planets embedded in disks.

Figs. 3a,b show the thermal emission from the simulated disks (seen face-on) with an embedded planet, which are to be compared with the available observational data on ϵ Eri and Vega shown in Figs. 3c,d (the parent stars are seen almost pole-on). There is a rather close resemblance between the observed and simulated disks (the central cavity may be masked by emission of dust from non-kuiperodal sources, such as comets). A smaller mass induces an asymmetric arc, with two clumps at its edges (Fig. 3a). A similar asymmetric structures has been revealed in sub-mm imagery of the ϵ Eri disk shown in Fig. 3c (Greaves

et al. 1998). A more massive planet makes the banana-like region more extended as well as merges two clumps into a single one (Fig. 3b). Such a planet may be responsible for an asymmetric feature in the simulated disk shown in Fig. 3b, which is reminiscent of the observed asymmetric north-east clump near Vega shown in Fig. 3d (Holland et al. 1998).

Using our modeling, we find that Vega may have a massive planet at a distance of $50 - 60$ AU, and ϵ Eri may have a less massive planet at a similar distance of $55 - 65$ AU. This conclusion is testable: Each resonant feature is stationary in the reference frame co-rotating with the planet, but it is not so for the observer at Earth. Therefore, if our interpretation of asymmetric clumps as a dynamical resonant structure is correct, the above asymmetric feature revolves around the star with an angular velocity of $1.2 - 1.6$ deg/year (Vega) and $0.6 - 0.8$ deg/year (ϵ Eri) - a prediction that can be tested within several years. If confirmed, the proposed interpretation of the structure in Vega- and ϵ Eri- like circumstellar disks seen face-on would make it possible not just to reveal the embedded planet and determine its semimajor axis, but also to constrain its other basic parameters, such as mass and eccentricity, and even to pinpoint the position of the planet (see Fig. 3a).

Although our simulations with just one planet qualitatively reproduce fairly well the observed structure of dusty disks in ϵ Eri and Vega, the quantitative details need further work. For instance, the present estimates for Vega's mass, 10 m_J, and ϵ Eri's mass, 0.8 m_J, (where m_J is Jupiter's mass) should be rather considered as upper limits. Indeed, the simulated structure varies with m_{pl}/β rather than with m_{pl} or β alone, and the actual value of β and therefore m_{pl} might be somewhat exaggerated. A more realistic e also tends to diminish m_{pl}. Collisions of dust particles, which act to populate as well as depopulate resonances, is an other factor which needs to be carefully accounted for. We expect that further detailed modelling of circumstellar disks in ϵ Eri and Vega would make possible to disentangle the basic parameters of the embedded planets.

In this *Letter*, we do not consider disks seen edge-on in scattered light, such as the β Pic disc revealed by STIS optical observations (Heap et al. 1999). Neither we discuss here dust rings, like HR 4796A or HD 141569, which are addressed elsewhere.

5. CONCLUSIONS

As we demonstrated above, a central 'hole' void of gas and dust as well as highly asymmetric structures in circumstellar disks can serve as indicators of planet(s) embedded in the disk. The major goal of the present *Letter* is to explore how the presence of the planet(s) impacts the disk, what particular resonances are responsible for the specific

asymmetric features in the dust, and how these features, shape of the disk, etc. would enable us to derive the major parameters of the yet invisible planetary system.

Numerical simulations described above lead to the following major conclusions:

1. The outermost planet in an exo-planetary system, which mass is $> 5 \cdot 10^{-5}\ M_\star$, can produce: (i) central cavity void of dust; (ii) a trailing (sometimes leading) cavity; and (iii) an asymmetric resonant dust belt consisting of arc(s) and one, two, or more clumps.

2. Morphology of these belts and cavities (size, asymmetry, number of clumps, and their pattern) depends upon β and particular resonances involved and is a strong function of the planetary mass, eccentricity of its orbit, and location of dust sources.

3. Asymmetry of resonant belts increases with mass of the planet. Amplitude of libration decreases with the planetary mass and β.

4. The crucial test of the above picture would be discovery of revolution of the resonant asymmetric structure around the star. For circumstellar disks in ϵ Eri and Vega the asymmetric design is expected to revolve by, respectively, $(0.6 - 0.8)^\circ$ and $(1.2 - 1.6)^\circ$ annually.

Numerical simulations described above present a method for determination of planetary parameters using a visible morphology of an outher part of circumstellar disk. We have demonstrated above that a very rich structure of the dusty disk with an embedded planetary system and its dependence upon the parameters of the planet and dust offer a possibility to reveal the presence of the planet(s) and to disentangle the planetary orbital parameters from dust parameters. Moreover, our high-resolution simulations ensure an opportunity to evaluate the major planetary characteristics, such as mass, semimajor axis and eccentricity.

The method of determining the planetary parameters using the shape and structure of the circumstellar disk is complementary to the current approaches of finding exo-solar planets using precise Doppler measurements, microlensing, and transits. Those approaches operate for Jupiter-like masses located close to the parent star so that the orbital period usually does not exceed several years. Our method yields information on planets including the outermost ones located at tens or hundreds of AU (i.e. with periods of several hundred years) and having variety of masses, both smaller and larger than Jupiter.

In sum, our modeling offers the ability to determine the major orbital parameters and masses of planets in dusty disks. As these disks are common, many planetary systems may be found. Moreover, since the dust disks are often so bright that they prevent direct detection of planets with imaging at visible, IR, or sub-mm wavelengths, our technique may actually be helpful in finding more planets than other methods do. It is well worth

the efforts to develop the modeling and interpretation for observations already available or obtainable in the near future.

REFERENCES

Beckwith, S.V.W., & Sargent, A.I. 1993, in *Protostars and Planets III*, ed. E.H.Levy & J.I.Lunine (Univ.of Arizona Press, Tucson), p. 521

Dermott, S.F., Jayaraman, S., Xu, Y.L., Gustafson, B.A.S. & Liou, J.C. 1994, Nature 369, 719

Gorkavyi, N.N., Ozernoy, L.M. & Mather, J.C. 1997, ApJ 474, 496

Gorkavyi, N.N., Ozernoy, L.M. & Mather, J.C. 1999 (to be submitted)

Gorkavyi, N.N., Ozernoy, L.M., Mather, J.C. & Taidakova, T. 1997, ApJ 488, 268 (GOMT)

Gorkavyi, N.N., Ozernoy, L.M., Mather, J.C. & Taidakova, T., 1999, Icarus (to be submitted)

Gorkavyi, N.N., Ozernoy, L.M., & Taidakova, T., 1999, Celestial Mechanics (to be submitted shortly)

Greaves, J.S., Holland, W.S., Moriarty-Schieven, G., Jenness, T., Dent, W.R.F., Zuckerman, B., McCarthy, C., Webb, R.A., Butner, H.M., Gear, W.K., & Walker, H.J. 1998, ApJ, 506, L133

Heap, S.A. et al. 1999, Ap. J., in press
(`http://oposite.stsci.edu/pubinfo/pr/1998/03`)

Holland, W.S., Greaves, J.S., Zuckerman, B., Webb, R.A., McCarthy, C., Coulson, I.M., Walther, D.M., Dent, W.R.F., Gear, W.K., & Robson, I. 1998, Nature, 329, p. 788

Jackson, A.A. & Zook, H.A. 1989, Nature 337, 629

Levison, H.F. & Duncan, M.J. 1997, Icarus 127, 13

Liou, J.C., Zook, H.A. & Dermott, S.F. 1996, Icarus 124, 429

Liou, J.-C. & Zook, H.A. 1997, Icarus, 128, 354

Marcy, G.W., Cochran, W.D., & Mayor, M. 1999, in *Protostars & Planets IV*, Eds. V. Manning, A. Boss, & S. Russell

Mather, J.C., Bely, P.Y., Stockman, P., & Thronson, H. 1997, in *Planets Beyond the Solar System and the Next Generation of Space Missions*. ASP Conf. Ser., v. 119, p. 245

Ozernoy, L.M. & Gorkavyi, N.N. 1999, ApJ (to be submitted) (OG)

Ozernoy, L.M., Gorkavyi, N.N.,& Taidakova,T. 1998, astro-ph/9812479; Icarus (submitted)

Roques, F., Scholl, H., Sicardy, B. & Smith, B.A. 1994, Icarus, 108, 37 and 59

Reach, W.T., Franz, B.A., Weiland J.L. et al. 1995, Nature, 374, 521

Taidakova, T. 1997, in *Astronomical Data Analyses, Software and Systems VI*, ed. G. Hunt & H.E.Payne, (San Francisco: ASP), ASP Conf. Ser. 125, p. 174

Taidakova, T.A. & Gorkavyi, N.N. 1999, in *The Dynamics of Small Bodies in the Solar Systems: A Major Key to Solar Systems Studies*, Eds. by B.A. Steves and A.E. Roy, NATO ASI Series, Series C. Mathematical and Physical Sciences, vol. 522, Kluwer Academic Publishers, p. 393.

TPF (Terrestrial Planet Finder). Origins of Stars, Planets, and Life. 1999, JPL/NASA, 158 pp.

Weidenschilling, S.J. & Jackson, A.A. 1993, Icarus 104, 244.

Wisdom, J. 1980, AJ 85, 1122

TABLE 1

Comparison of Our Approach With That of RSSS[1]

	RSSS	Our approach
ımber of particles in the grid	8192	10^{10-11}
ety of resonances accounted for	a few low-order resonances	all mean motion resonances
televance to planetary disks	particles of the same age	particles of all ages
) Computationals errors and integrator stability	4th order Runge-Kutta integrator with single precision	implicit 2nd order Potter's method with double precision [2,3]
Constraints on time scale of evolution, τ_{evol}	$\tau_{evol} < 10^4$ revolutions of the planet [4]	$\tau_{evol} < 2 \cdot 10^6$ revolutions of the pla
6) Computing facility, CPU time	Connection machine CM 2/8k, 6 hrs	several PCs a few to a few tens hrs
No. of different variants	9	40
ange of planet's mass	$10^{-3}\ m_J \lesssim m_{pl} \lesssim 0.15\ m_J$	$0.05\ m_J \lesssim m_{pl} \lesssim 10\ m_J$
ıparability with observations	no disk emission considered	disk emission considered

[1] Roques, Scholl, Sicardy & Smith (1994)

[2] Taidakova (1997)

[3] Taidakova & Gorkavyi (1997)

[4] RSSS neglected 20% of long-living resonant particles

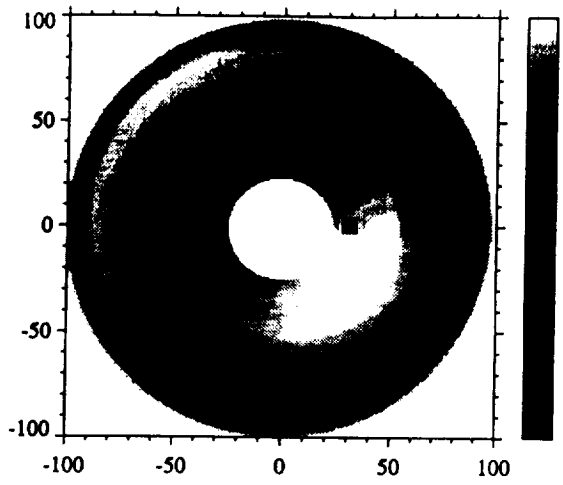

1a) M=0.3 M_J, 3:1, β=0.065, t_{res}=8x10^5

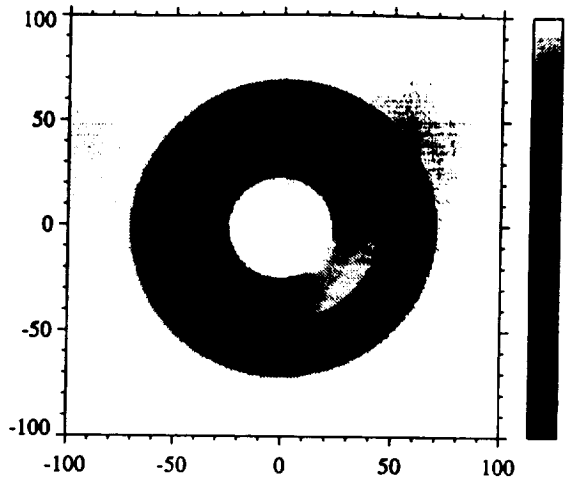

1b) M=0.3 M_J, 2:1, β=0.065, t_{res}=2.4x10^5

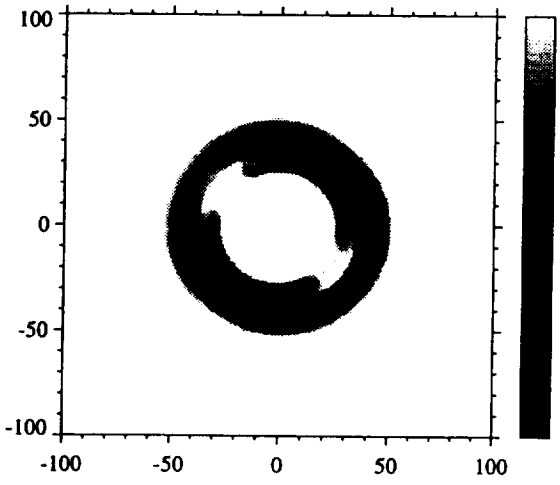

1c) M=0.3 M_J, 3:2, β=0.065, t_{res}=5x10^4

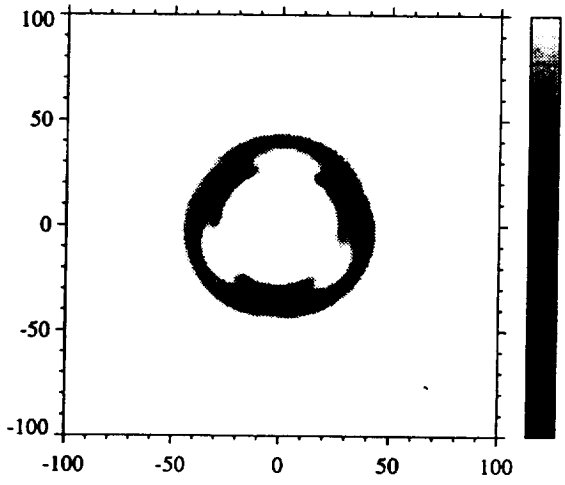

1d) M=0.3 M_J, 4:3, β=0.065, t_{res}=2x10^4

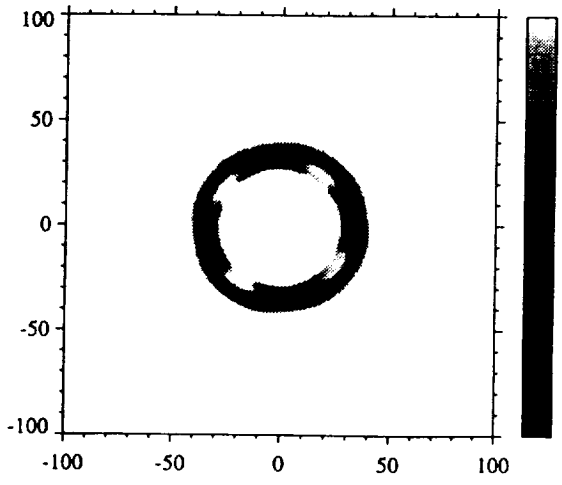

1e) M=0.05 M_J, 5:4, β=0.02, t_{res}=7x10^4

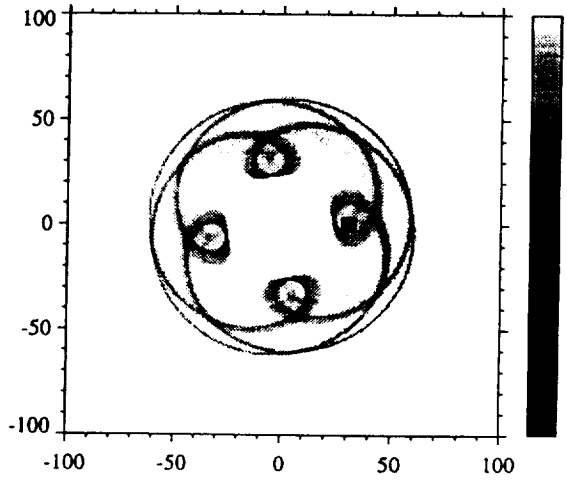

1f) M=0.1 M_J, 7:4, β=0.02, t_{res}>10^6

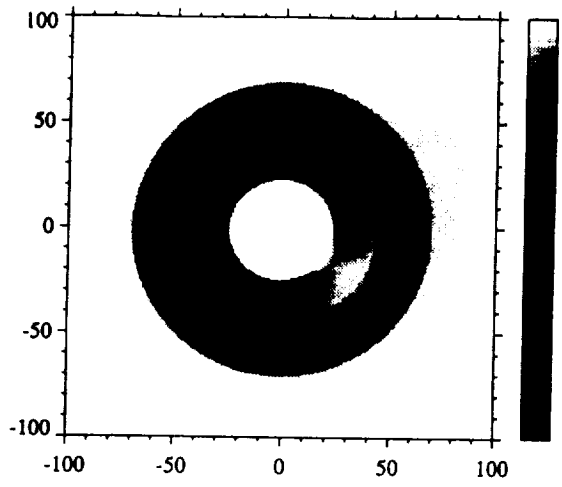

2a) M=0.05 M_J, 2:1, β=0.065, t_{res}=2.3x10^5

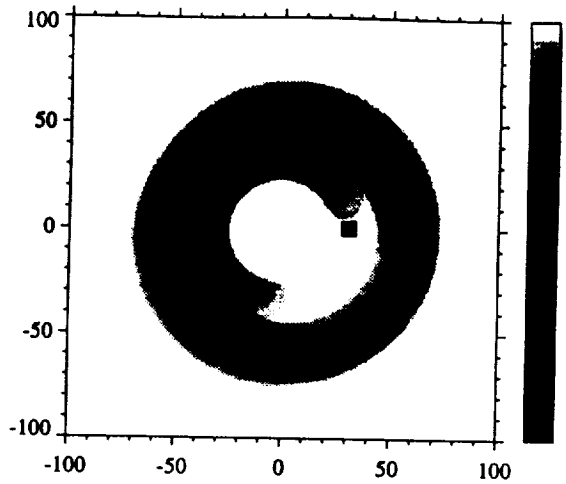

2b) M=5 M_J, 2:1, β=0.065, t_{res}=1.6x10^5

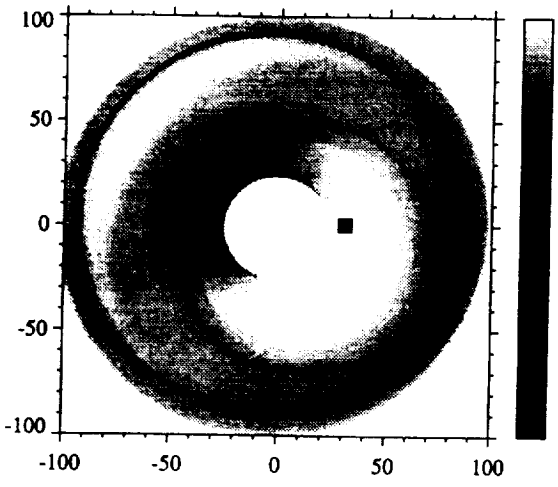

2c) M=5 M_J, 3:1, β=0.065,t_{res}=6.8x10^5

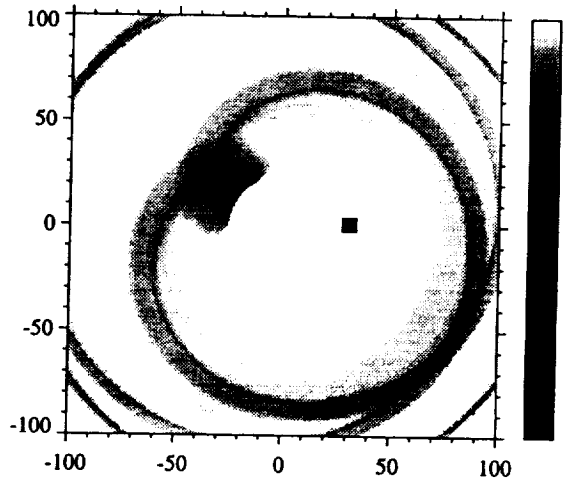

2d) M=5 M_J, 4:1, β=0.04, t_{res}>2x10^6

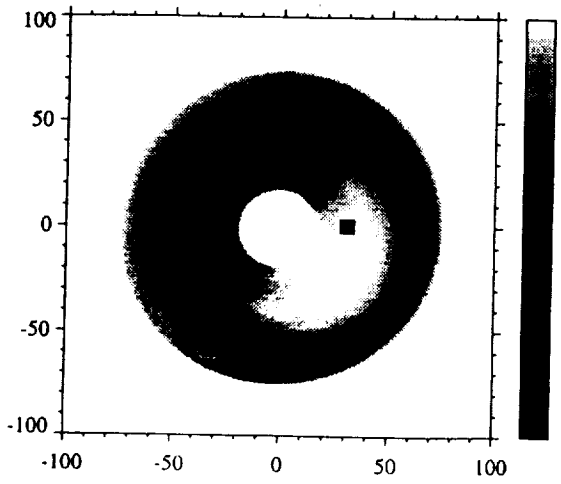

2e) M=0.3 M_J, 2:1, β=0.065, t_{res}=2.3x10^5

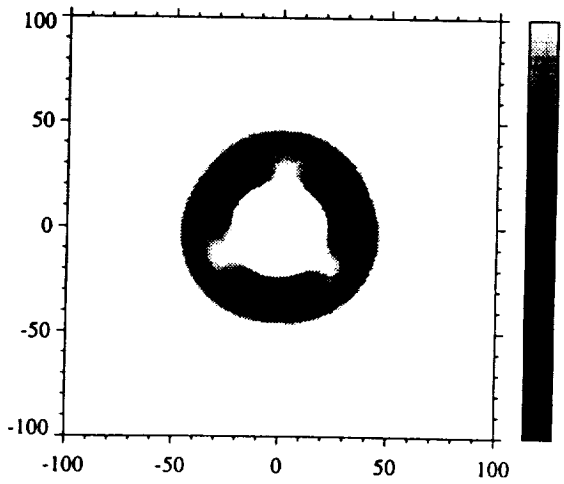

2f) M=0.3 M_J, 4:3, β=0.065, t_{res}=7x10^4

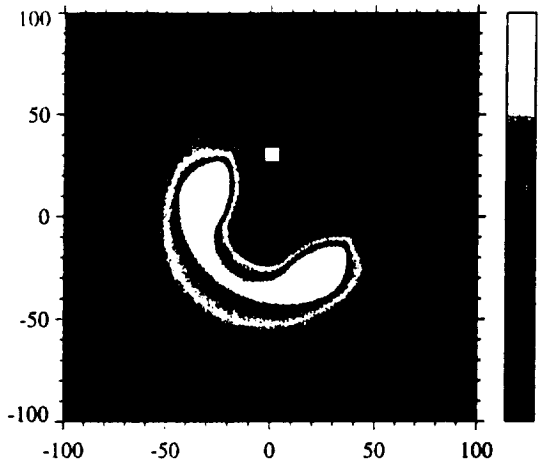

3a) M=0.8 M_J, 2:1, β=0.065, t_{res}=3.4x10^5

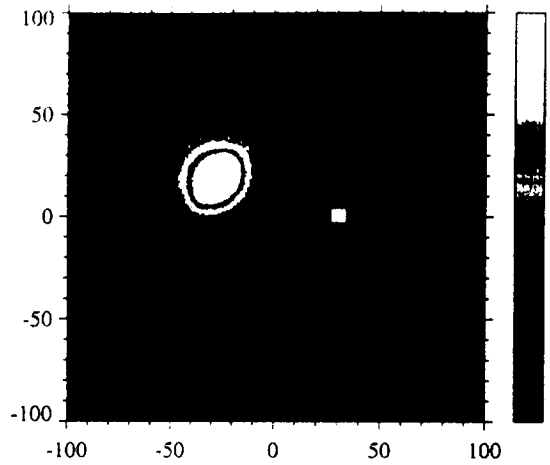

3b) M=10 M_J, 4:1, β=0.065, t_{res}=1.9x10^6

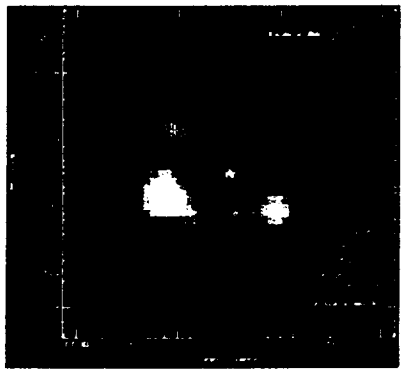

3c) ε Eri (SCUBA Observation)

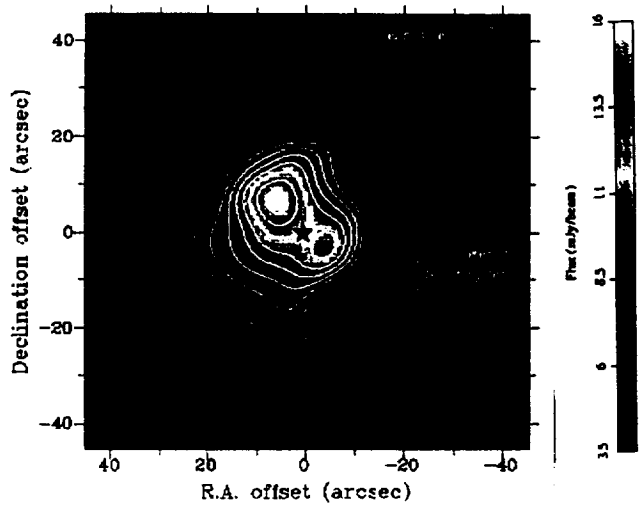

3d) Vega (SCUBA Observation)